Performance Evaluation of a Residual Stress Measurement Device Using Indentation and a Radial In-Plane ESPI Interferometer

Ricardo Suterio [a,b], Armando Albertazzi G. Jr [b], Felipe Kleber Amaral [b], Anderson Pacheco [b]

[a] Integration and Tests Laboratory (LIT), National Institute for Space Research (INPE)

[b] Metrology and Automation Laboratory (Labmetro), Federal University of Santa Catarina (UFSC)
Cx. Postal 5053, CEP 88040-970, Florianópolis, SC, Brasil
albertazzi@labmetro.ufsc.br

ABSTRACT

A radial in-plane electronic speckle pattern interferometer (ESPI) is used to measure residual stresses in combination with an indentation method. A semi-empirical mathematical model is developed to quantify the residual stresses from the radial in-plane displacement component measurement around the indentation print. Several tests were made in a specimen with different levels of residual stresses induced by mechanical loading. Correlation functions were fitted to tests results and are used to predict the residual stresses levels. This paper briefly presents the measurement principle, testing details and results of the performance evaluation. Finally, an uncertainty budget of the testing and measurement process was carried out. The tests presented here are not complete since they are restricted to only one material, one-axis stress state, two indentation tip geometry and only one indentation force, but they are sufficient to encourage further development.

Keywords: residual stress, indentation, ESPI; radial interferometer.

INTRODUCTION

There are a large number of engineering applications where residual stresses are present and can strongly influence the behavior or life of a mechanical component. Manufacturing processes like welding, casting, stamping, forging usually induce an expressive amount of residual stresses. Since the residual stresses state is very difficult to be predicted by analytical or numerical methods, they are frequently measured.

Unfortunately it is not easy to measure residual stresses. There are an expressive number of experimental methods, but only few of them are of practical interest or metrologicaly reliable. One of the most widely used experimental methods is the hole-drilling technique. This technique involves monitoring the strains produced when a small hole is drilled into a stressed material. The drilled hole produces a local release of residual stresses that are measured by a special type of strain gauges. Those values are used into an appropriate mathematical method to quantify the residual stresses level[4].

A radial in-plane electronic speckle pattern interferometer (ESPI) has been developed by the authors' group using conical mirrors.[1] True radial in-plane sensitivity is achieved in a circular measurement area. This device has been used for several applications on the field of experimental mechanics, including with the hole drilling method for residual stresses measurement[7],[8],[9],[10]. In this paper this radial in-plane (RIP) is used, in combination with an indentation method, to measure residual stresses[6].

The measurement principle consists of applying a controlled indentation print to the surface of the specimen by a conical or spherical tip. As a consequence, a local yielding is developed and the material on the specimen surface moves away from the indentation print. In opposition to the hole drilling method, the indentation does not release stresses but add more stresses creating a local plastic zone. The amount of the radial displacement component around the indentation print is influenced by the level and direction of residual stresses state acting on the specimen. By measuring the radial displacement field around the indentation print and fitting it in an appropriate mathematical model, it is possible to

763

obtain quantitative information that the authors want to use to infer the amount of residual stresses present on mechanical parts.

Since there are not available in the market standards with a well established reference value for residual stresses, it is very difficult to calibrate and to assure the performance of a residual stresses measuring device. A mechanical device is used in this work to produce a reference value for testing the residual stresses measurement device. The performance evaluation of the mechanical loading device and residual stresses measurement technique are analyzed through an uncertainty budget.

THE RADIAL IN-PLANE INTERFEROMETER

A double illumination radial in-plane electronic speckle pattern interferometer (RIP-ESPI) is used in this paper[1],[6]. The basic principle is shown in Figure 1. A collimated laser beam is vertically directed toward a set of two conical mirrors. The reflected beams form a double illumination on the specimen surface. It can be verified that true in-plane radial sensitivity is achieved. A practical configuration of the radial in-plane interferometer is shown in Figure 1(b). The laser light is expanded and collimated. The collimated beam is reflected towards the conical mirror using a 45° flat mirror. The central circular window located at this 45° mirror has two main functions: (a) to avoid that the laser light to reach directly the measured surface to prevent triple illumination, and (b) to provide a viewing window for the camera. The conical mirror is formed by two parts with a small gap with value is controlled by a PZT actuator do produce phase shifting. This interferometer was recently incorporated in a portable and modular device for residual stresses measurement.
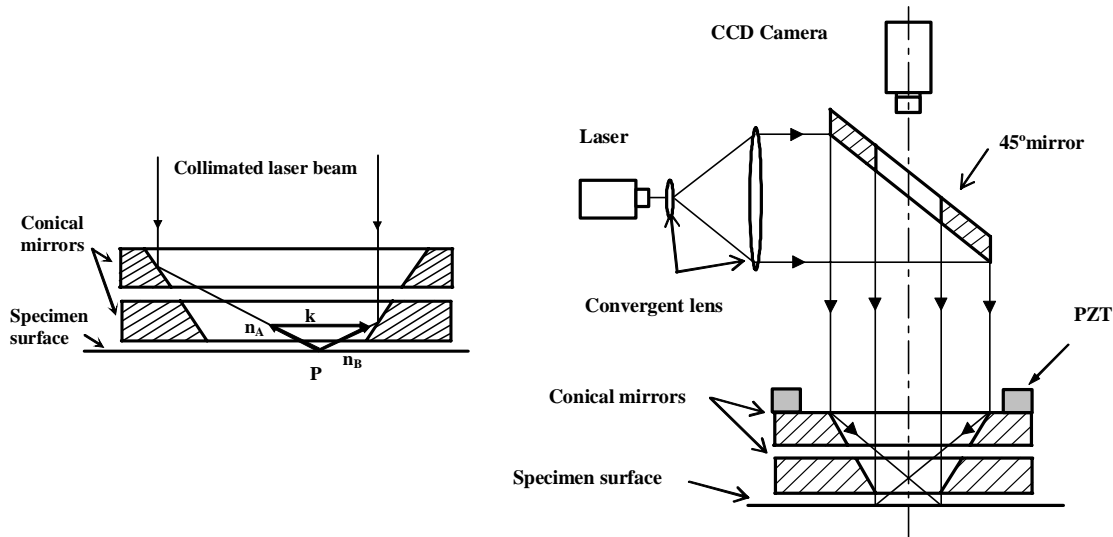

Figure 1: Double illumination through the radial interferometer. [1]

RESIDUAL STRESS MEASUREMENT

In order to quantify residual stresses with the RIP-ESPI at least two different stages are involved. First, a reference set of images of the specimen's surface is acquired and the correspondent phase of the double illuminated speckle pattern is computed. Then, the stress state is changed by hole-drilling or by indentation. After that, a second set of images of the same region is acquired and the speckle phase computed again. Finally, the phase difference pattern with quantitative information about the radial in-plane displacement component is obtained. Figure 2(a) shows a typical phase difference pattern with radial sensitivity for a one-axis residual stress state due to hole-drilling method. The hole diameter was 1.6 mm and the induced residual stress level was about 200 MPa.

By the other hand, when indentation is used, the local stresses are not released, but more stresses are added, producing a local yielding. As a consequence, a permanent displacement field is produced around the indentation print. In a stress-free material, this permanent displacement field is axi-symmetrical and repeatable if the indentation tip geometry, indentation loading and material properties are constant. Figure 2(b) shows the resulting pattern of stress-free steel indented by a 120° conical tip. If mechanical or residual stresses are present in the material prior the indentation, the permanent displacement field is affected in a way that depends on the residual stresses levels. Figure 2(c) shows the radial displacement in a material with a one-axis 200 MPa stresses field aligned about 30° with the horizontal axis. There are clear differences.

If one subtracts the phase difference pattern of Figure 2(c) minus Figure 2(b) only the effects of residual stresses remains on the image. The resulting pattern is shown in Figure 2(d). It is possible to see some similarity between Figure 2(a) and Figure 2(d). That similarity inspired the development of the mathematical model used in this work.
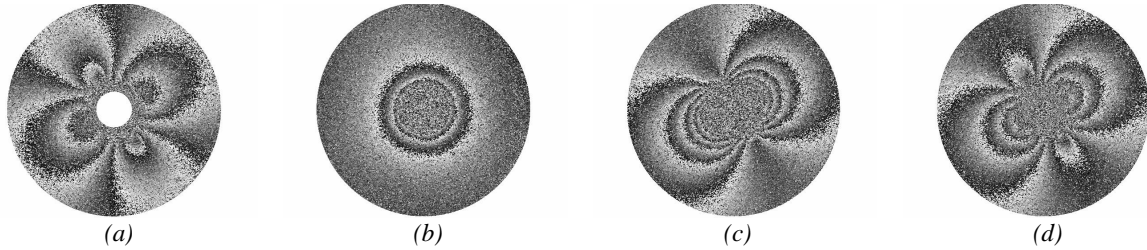

(a)   *(b)*   *(c)*   *(d)*

Figure 2: Typical phase patterns of the radial displacement fields component:
(a) for holing drilling method (computer simulated), (b) in a stress-free material after indentation,
(c) with 200 MPa stress after indentation, and (d) phase difference: (c - b)

MATHEMATICAL MODEL

A mathematical model for residual stresses measurement with indentation was derived starting from the hole-drilling method model show in equation (1). It is noted that the term that depend on $cos(2\theta)$ is related to the principal stresses difference $(\sigma_1 - \sigma_2)$ and the term independent of θ is related to the principal stresses sum $(\sigma_1 + \sigma_2)$. The radial component of the displacement field (u_r) was proposed by the authors[6],[7],[8], is here modeled in polar coordinates by the following equation:

$$u_r(r,\theta) = \frac{(1+\upsilon)}{2E}\frac{1}{r}K_1 + \frac{2}{E}\frac{1}{r}K_2 \cos(2\theta - 2\beta) \qquad (1)$$

where

u_r	is the radial displacement component
r, θ	are polar coordinates
v, E	are material's Poisson ratio and Young modulus respectively
σ_1, σ_2	are the principal residual stresses components
β	is the principal angle of stresses

K_1 and K_2 are unknown functions given by:

$$K_1 = H[(\sigma_1 + \sigma_2), \psi] \qquad\qquad K_2 = \Gamma[(\sigma_1 - \sigma_2), \psi] \qquad (2)$$

and ψ was defined as equivalent indentation diameter.

It was experimentally verified that the radial displacement field resulting of an indentation print on a stress-free material can be reasonably described using the equation proposed by Giannakopoulos & Suresh - 1997: [2]

$$u_r(r) = K_3 \frac{\upsilon}{E(\upsilon-1)} \frac{1}{r^{\frac{1}{\upsilon}-1}} \qquad (3)$$

K_3 is a constant that depends upon the indentation force, tip geometry and materials properties.

For a given material, indentation tip geometry and material properties the constant K_3 can be determined by fitting equation (3) to experimental data. So, the complete model becomes:

$$u_r(r,\theta) = \frac{(1+\upsilon)}{2E} \frac{1}{r} K_1 + \frac{2}{E} \frac{1}{r} K_2 \cos(2\theta-2\beta) + \frac{\upsilon}{E(\upsilon-1)} \frac{1}{r^{\frac{1}{\upsilon}-1}} K_3$$

$$(4)$$

The experimental data is fitted to this model and values are determined for K_1, K_2. K_3 remain constant if the material and indentation conditions are the same. K_1 is a function of $(\sigma_1 + \sigma_2)$ and K_2 is a function of $(\sigma_1 - \sigma_2)$.

EXPERIMENTAL SETUP

Figure 3(a) shows the portable ESPI radial in-plane interferometer used in this work. Four modules are available: from left to right a hole-drilling module, the universal clamping base and the measurement head. The measurement head is equipped with a diode laser with 658 nm wavelength, a conical mirror and a CCD camera. The double illuminated region is about 10 mm in diameter. Figure 3(b) shows the indentation module, which is equipped with a mechanical indentation device that always applies the same level of constant impact energy. Two different tip geometries were used: a 120° conical diamond tip and a 2.5 mm diameter spherical tungsten carbide tip.
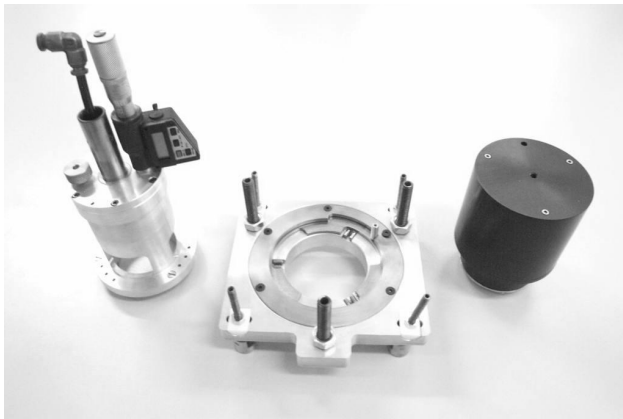

*(a) Hole-drilling module, universal base, and radial in-plane interferometer.*
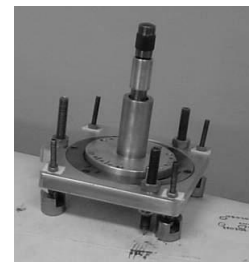
(b) Indentation module with a 120° conical diamond or a 2.5 mm diameter spherical tungsten carbide tips

Figure 3: Portable ESPI radial in-plane interferometer used in this work.

To evaluate the measurement performance of a residual stresses measurement device, the authors applied a known mechanical stresses level in a previously annealed specimen. That approach mechanically simulates a residual stresses state with some uncertainty. The mechanical loading device is shown in Figure 4(a). Basically, a long residual-stresses free specimen is loaded by traction through 6 bolts connected to a "U" shaped structure. The specimen is a rectangular AISI 1020 steel bar with approximate dimensions of 3 x 50 x 3000 mm (Figure 4b). The long specimen was instrumented with ten strain gages to monitoring the actual tension level applied to the specimen in order to guarantee uniform loading and to provide a reference value for it. The specimen size is long enough to accommodate over 300 measurement points. The portable radial in-plane interferometer was clamped to the loading device in such a way that its measurement axis was always aligned in about 30° with the loading direction.
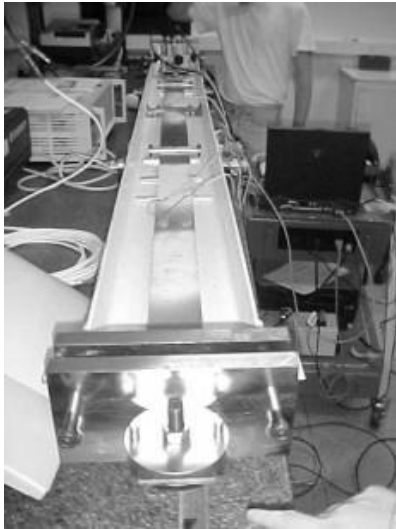
(a) Mechanical system used for simulating
a known residual stresses state
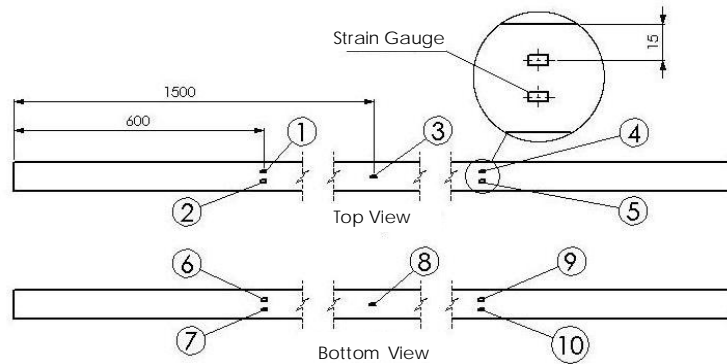
(a) Instrumented specimen and configuration of the ten strain gauges

Figure 4: Loading system, specimen, and strain gages configuration.

EXPERIMENTAL RESULTS

A set of measurement tests was planned and executed with nine different stresses levels. Both 120° conic tip and 2.5 mm spherical indentation tips were used applying about the same amount of energy given by mechanical impact of a projectile driven by a spring at constant compression rate. Each experiment was repeated three times.

Figure 5(a) to Figure 5(d) show different experimentally obtained images. A 30° rotated 177 MPa one-axis stresses filed was applied in the long specimen. Both indentation tips geometry were used. Figures 5(a) and (c) are the total displacement fields after indentation. Figures 5(b) and (d) are the difference displacement pattern resulting after subtracting the stress-free displacement field. In this paper only the performance evaluation results from total displacement fields are reported.
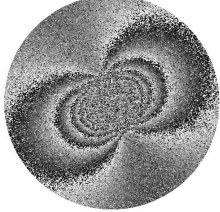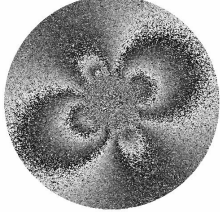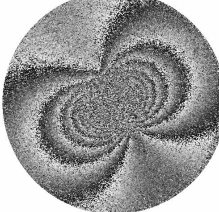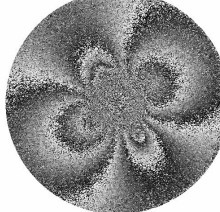
Test at 177 MPa, 120° conical tip		*Test at 177 MPa, 2.5 mm spherical tip*	
(a) total phase difference after indentation in a loaded material.	(b) phase difference: loaded material minus a stress-free material.	(c) total phase difference after indentation in a loaded material.	(d) phase difference: loaded material minus a stress-free material.

Figure 5: Typical test results for two indentation tips in a 30° rotated one-axis stress field.
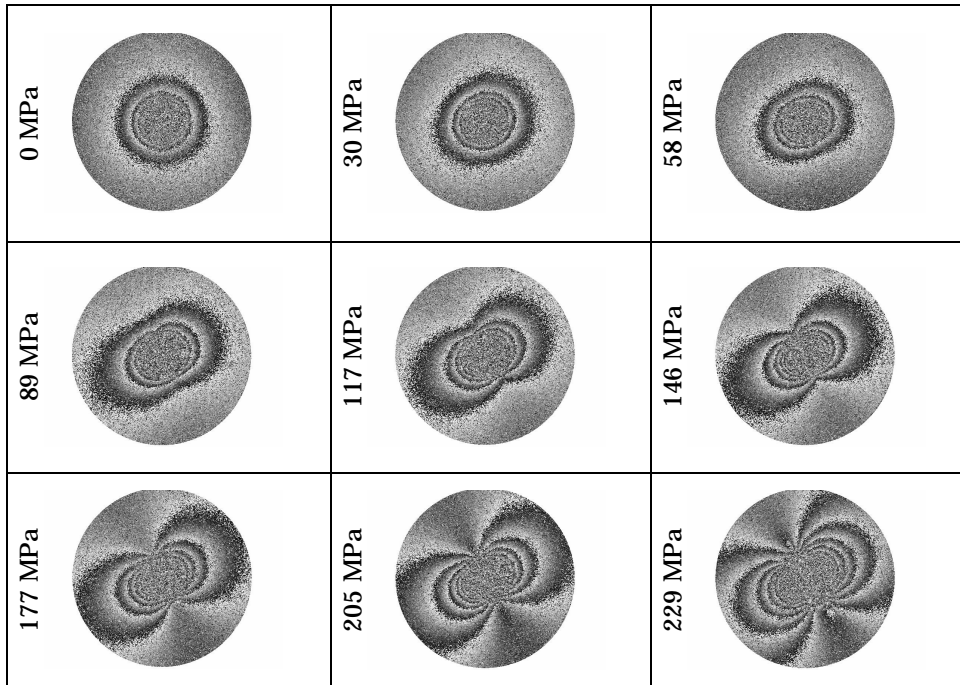
Figure 6: Images from conical indentation versus induced residual stress

Figure 7: Images from spherical indentation versus induced residual stress

Figure 6 show the images obtained from conical indentation. The induced residual stresses levels are indicated. They range from 0 to 229 MPa, equivalent to 0 to 80 % of the material's yield stress. Figure 7 is for spherical indentation. The reference values for residual stresses were computed from the mean value of the strain gauges. The uncertainty for the

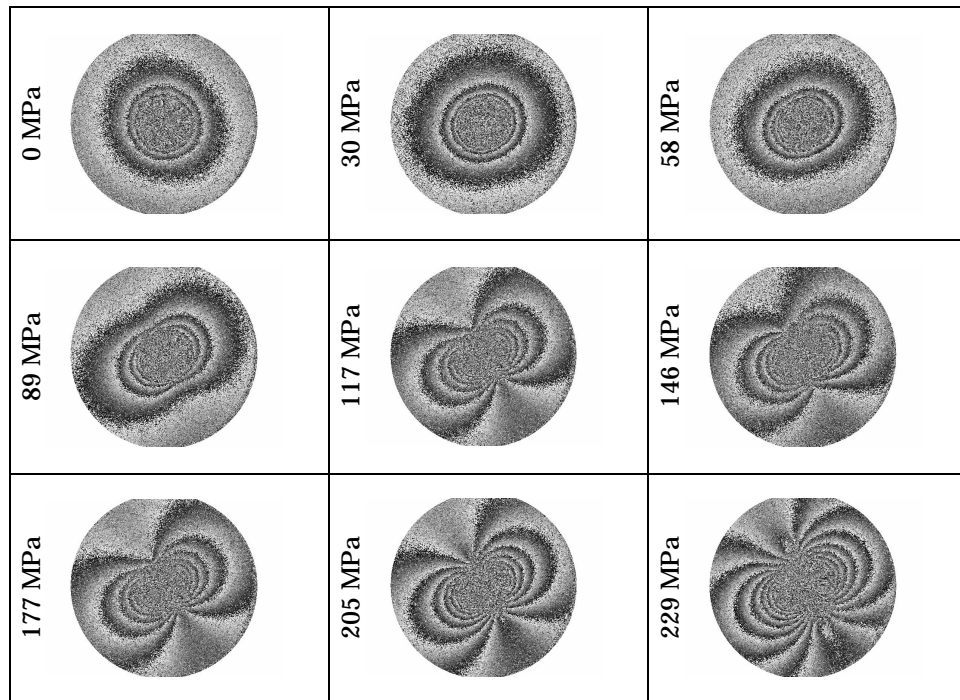stress induced level was from 5 to 9% with 95% confidence level[9]. The sampling region was delimited by two concentric circles with minimum radius of 1.7 mm for conical indentation and 2.0 mm for spherical indentation and maximum radius of 4.5 mm for both. A polar mesh of 12 x 360 = 4320 sampling points was used in all cases.

Table 1 and Table 4 present measurement results. Columns one and two present the reference stress level in MPa and relative to material's yield stress. The mean value of parameters K_1, K_2 and K_3, fitted by least squares are presented next.

Figure 8 and Figure 9 plot the experimental relation between K_1, K_2 and the reference stress level. Two quadratic polynomials, $H(K_1) = K_1$ versus $(\sigma_1+\sigma_2)$ and $\Gamma(K_2) = K_2$ versus $(\sigma_1-\sigma_2)$, were fitted to the experimentally computed values, as show in Table 3. In this particular case both sum and difference of principal stresses are equal since $\sigma_2 = 0$. K_3 did not show a correlation with the applied stresses. Its value is more correlated to the indentation energy that, ideally, was kept constant. Quadratic polynomial regression shows a quite good agreement with experimental data (see Table 3).

σ_1 and σ_2 can be computed by: $\sigma_1 = (H + \Gamma) / 2$ and $\sigma_2 = (H - \Gamma) / 2$. The resulting computed values for σ_1 and σ_2 are presented in Table 2.

Table 1: Parameters K_1 trough K_3 determined using least square fitting for 120° diamond cone tip.

σ_{ref} [MPa]	σ_{ref} / σ_y [%]	K_1	K_2	K_3
0.0	0.0%	60.04	8.08	-597
29.8	10.1%	136.88	11.14	-617
58.1	19.7%	123.60	17.72	-609
89.2	30.2%	161.29	32.97	-615
116.9	39.6%	194.78	51.58	-728
145.7	49.4%	203.40	67.09	-655
177.3	60.1%	236.76	82.58	-637
205.0	69.5%	314.01	111.67	-688
229.3	77.7%	428.63	150.00	-797
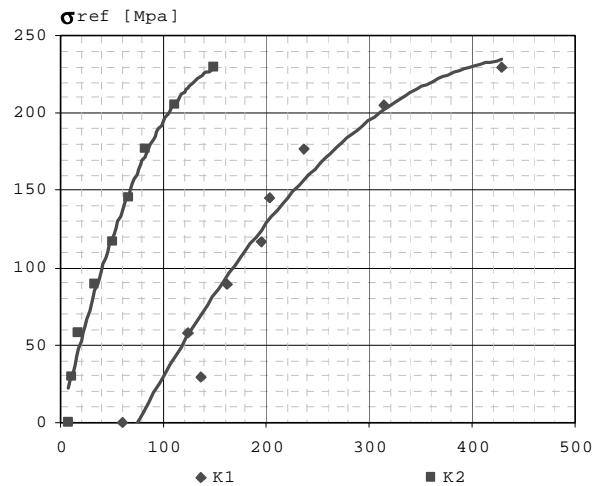
Figure 8: Indentation parameter versus reference residual stress for 120° diamond cone tip.

Table 2: Predict stresses values for a 120° diamond cone tip.

Ref. Value [MPa]	Relative to Yield Point	Predict Values		Deviation	
σ_{ref} [MPa]	σ_{ref} / σ_y	σ_1 [MPa]	σ_2 [MPa]	$\sigma_{ref} - \sigma_1$ [MPa]	$(\sigma_{ref} - \sigma_1) / \sigma_{ref}$
0.0	0.0%	1.8	-20.2	1.8	--
29.8	10.1%	50.1	20.0	20.2	67.8%
58.1	19.7%	51.5	4.7	-6.6	-11.4%
89.2	30.2%	88.5	5.7	-0.7	-0.8%
116.9	39.6%	122.9	1.4	6.0	5.2%
145.7	49.4%	140.4	-8.9	-5.4	-3.7%
177.3	60.1%	164.9	-8.0	-12.4	-7.0%
205.0	69.5%	204.4	-2.1	-0.6	-0.3%
229.3	77.7%	231.7	2.7	2.4	1.0%

Table 3: Quadratic polynomials fitted to the experimentally computed values H(K₁) and Γ(K₂)

120° conical tip	2.5 mm spherical tip
$H(K_1) = -0.001595\ K_1^2 + 1.4653\ K_1 - 100.61$ ($R^2 = 0.946$)	$H(K_1) = -0.0009301\ K_1^2 + 1.2604847\ K_1 - 195.8968010$ ($R^2 = 0.992$)
$\Gamma(K_2) = -0.008430\ K_2^2 + 2.7906\ K_2$ ($R^2 = 0.986$)	$\Gamma(K_2) = -0.0033273\ K_2^2 + 1.8136312\ K_2$ ($R^2 = 0.992$)

Quadratic regression for the 2.5 mm diameter tungsten carbide spherical tip shows a better agreement with experimental data. The correlations of *H* and *Γ* functions are better than 0.99 (R^2), see Table 3. Also here, from those predicted values, σ_1 and σ_2 can be computed by: $\sigma_1 = (H + \Gamma) / 2$ and $\sigma_2 = (H - \Gamma) / 2$.

The resulting computed values for σ_1 and σ_2 are presented in Table 5.

Table 4: Parameters ψ_1 trough ψ_3 determined using least square fitting for 2.5 mm diameter tungsten carbide spherical tip.

σ_{ref} [MPa]	σ_{ref} / σ_y [%]	K_1	K_2	K_3
0.0	0.0%	192.08	6.82	-895
29.8	10.1%	214.75	13.37	-926
58.1	19.7%	262.53	26.99	-883
88.7	30.1%	283.08	56.11	-924
116.9	39.6%	346.49	79.05	-1021
145.8	49.4%	374.10	103.12	-859
177.1	60.0%	414.81	123.42	-791
204.8	69.4%	490.54	155.14	-746
228.7	77.5%	664.09	201.87	-761
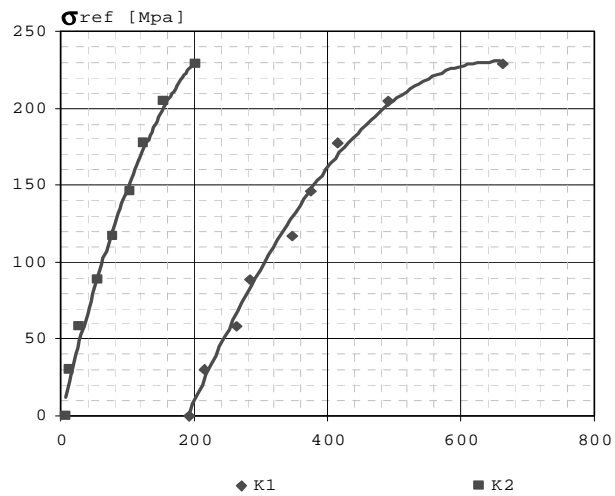
Figure 9: Indentation parameter versus reference residual stress for 2.5 mm diameter tungsten carbide spherical tip.

Table 5: Predict stresses values for a 2.5 mm diameter tungsten carbide spherical tip.

Ref. Value [MPa]	Relative to Yield Point	Predict Values		Deviation	
σ_{ref} [MPa]	σ_{ref} / σ_y	σ_1 [MPa]	σ_2 [MPa]	$\sigma_{ref} - \sigma_1$ [MPa]	$(\sigma_{ref} - \sigma_1) / \sigma_{ref}$
0.0	0.0%	6.6	-5.5	6.6	--
29.8	10.1%	23.3	-0.2	-6.5	-21.8%
58.1	19.7%	56.1	9.8	-2.0	-3.4%
88.7	30.1%	86.9	-4.1	-1.8	-2.0%
116.9	39.6%	125.6	3.4	8.7	7.5%
145.8	49.4%	148.9	-2.4	3.1	2.1%
177.1	60.0%	171.0	-1.8	-6.1	-3.4%
204.8	69.4%	201.5	0.5	-3.4	-1.6%
228.7	77.5%	230.3	-0.1	1.6	0.7%

UNCERTAINTY ANALYSES

The ideal performance evaluation of a measurement device requires a well known reference value. The difference between the measured value and the reference value is the measurement error. The uncertainty of the induced residual stresses values computed from strain gauges is not good enough to be considered as a reference. So, the best one can do is to compute the deviation between both values and the uncertainty components of this deviation. That is not a complete performance analysis, but it gives some valuable information about the overall performance.

Two groups of uncertainty sources were considered: related to the residual stresses induction and to the optical measurement system. An uncertainty budget is presented in Table 6. In this case the mechanically induced residual stress was 177.1 MPa and a spherical indentation tip was used.

The goal of the residual stresses induction device is to produce a known uniform one-axis residual stresses state. But this goal is not reached due to several disturbing factors. The upper part of Table 6 presents the seven most expressive error sources and also their estimated standard uncertainties. The loading device is not capable to apply a uniform stress state to the entire long specimen by itself due to mechanical limitations and to specimen imperfections. So, six adjusting bolts are used to apply the closest possible stress distribution. The stresses values are monitored by a set of ten strain gauges. At the end, the readings of the ten strain gauges are close, but they are not the same. The standard deviation of the ten different readings of the strain gauges is far the most expressive uncertainty source. The preexisting residual stresses in the specimen are the second major error source in importance. After combining the influence of all these seven error sources, the expanded uncertainty (with 95% confidence level) for residual stresses induction is $\pm$ 17.2 MPa or $\pm$ 9.7% of the applied residual stresses.

The second group of uncertainties is related to the optical measurement system itself. Sixteen error sources were considered. The dispersion for the fitted value for K_1 is the major uncertainty source. This dispersion was obtained by repeating the measurement tests with same loading. It is influenced by the amount of energy applied by the indentation device, by material's local non homogeneities and by the capability of the loading device to repeat the same level of stress. The variability of K_2 is a lot smaller than K_1. It means that the developed system is a lot better to compute the differences of residual stresses then to its mean value. After combining all the factors, the resulting expanded uncertainty for optical measurement system reaches $\pm$ 28.8 MPa or $\pm$ 16.2% of the applied residual stresses.

Figure 10 show graphically the contribution of each factor. The expanded uncertainties are presented with 95% confidence level. Important conclusions can be gotten:

- The biggest uncertainty source is coming from K_1. Apparently the mathematic model is very sensitive to the repeatability of the amount of applied energy to the indentation that is not conveniently absorbed by K_3.

- The second one is due the non uniform state of stresses applied to the specimen that produces differences in the strain gauges readings. This confirms that the loading device is not good enough. It must be seen that this uncertainty source also has an effect on the previous one.

- A better knowledge of the material's properties also is a factor that would improve the total uncertainty.

- The uncertainties related to the radial interferometer itself, such as the image scale factor, laser wave length variation, conical mirror irregularities and camera aspect ratio, had been improved simply by a laboratory calibration.

The results presented on Table 6 and Figure 10 are relative to the longitudinal principal stresses of the specimen. By combining both uncertainty groups, the overall measurement uncertainty is something around $\pm$34 MPa for 177 MPa. It must be clear that part of this uncertainty comes from the imperfections of the loading device. In practice this result are quite good and comparable with other residual stress measurement methods.

Table 6: Uncertainty budget of the measurement system: Indentation in steel and spherical indentador

	Uncertainty sources	Measurement / Specification						Random effects				
Symbols	Description	Estimative	Unit	Estimate value	Unit	Measurement	Distribution probability	sensitivity coefficient	Unit	Divisor	Standard uncertainty [MPa]	Degree of freedom
	Residual Stresses Induction											
x1	Strain reading error	885.60	μm/m	36.56	μm/m	10	normal	0.2	MPa/μm/m	1.00	7.312	9
x2	Zeror error	1.00	μm/m	1.00	μm/m	--	rectangular	0.2	MPa/μm/m	1.73	0.115	∞
x3	Amplifier uncertainty	0.20	%	1.77	μm/m	--	rectangular	0.2	MPa/μm/m	1.73	0.205	∞
x4	Gauge factor	1.00	%	8.86	μm/m	--	rectangular	0.2	MPa/μm/m	1.73	1.023	∞
x5	Gauge positioning error	1.00	°	0.13	μm/m	--	rectangular	0.2	MPa/μm/m	1.73	0.015	∞
x6	Preexisting residual stresses	15.00	μm/m	15.00	μm/m	--	rectangular	0.2	MPa/μm/m	1.73	1.732	∞
x7	Mechanical properties variability	0.20	%	1.7712	μm/m	--	rectangular	0.2	MPa/μm/m	1.73	0.205	∞
				expanded uncertainty for inducted residual stresses:						**17.2 MPa**		**9.7%**
	Measurement System											
x8	K1 variability ($\sigma 1 + \sigma 2$)	51.11	--	10.88	MPa	4	normal	1	MPa	1.00	10.880	3
x9	K2 variability ($\sigma 1 - \sigma 2$)	6.46	--	2.98	MPa	4	normal	1	MPa	1.00	2.980	3
x10	K4 energy load variability	17.60	%	0.01	MPa	4	normal	1	MPa	1.00	0.010	3
x11	Numeric errors	1.00	%	1.77	MPa	--	rectangular	1	MPa	1.73	1.023	∞
x12	"x" image center error	3.00	pixel	0.05	MPa	--	rectangular	1	MPa	1.73	0.029	∞
x13	"y" image center error	3.00	pixel	0.13	MPa	--	rectangular	1	MPa	1.73	0.075	∞
x14	Young's module error	6.00	GPa	4.06	MPa	--	rectangular	1	MPa	1.73	2.344	∞
x15	Poisson's coefficient error	0.02	--	8.02	MPa	--	rectangular	1	MPa	1.73	4.630	∞
x16	Image scale factor	0.00005	mm/pixel	0.75	MPa	15	normal	1	MPa	1.00	0.750	14
x17	Laser and conic mirror errors	2.50	%	4.2	MPa	--	rectangular	1	MPa	1.73	2.425	∞
x18	Camera aspect ratio	0.10	%	0.7	MPa	--	rectangular	1	MPa	1.73	0.404	∞
x19	Effect of internal radius positioning	0.50	mm	0.39	MPa	--	rectangular	1	MPa	1.73	0.225	∞
x20	Effect of external radius positioning	0.50	mm	0.65	MPa	--	rectangular	1	MPa	1.73	0.375	∞
x21	Rigid body displacement ("x" translation)	1.00	μm	0.07	MPa	--	rectangular	1	MPa	1.73	0.040	∞
x22	Rigid body displacement ("y" translation)	1.00	μm	0.09	MPa	--	rectangular	1	MPa	1.73	0.052	∞
x23	Image optical noise	--	--	0.32	MPa	--	rectangular	1	MPa	1.73	0.185	∞
	Total			**expanded uncertainty for the measurement system:**						**28.8 MPa**		**16.2%**
	measured stress:	**177.1 MPa**										

The uncertainties evaluations for σ_2 are in the order of ±15 MPa for the same confidence level.

By the other hand, the measurement system presented a remarkably better performance to determine the principal stresses directions (β), for stresses superior to 20 % of the material yield point. The typical uncertainties are always inferior ± 1°.
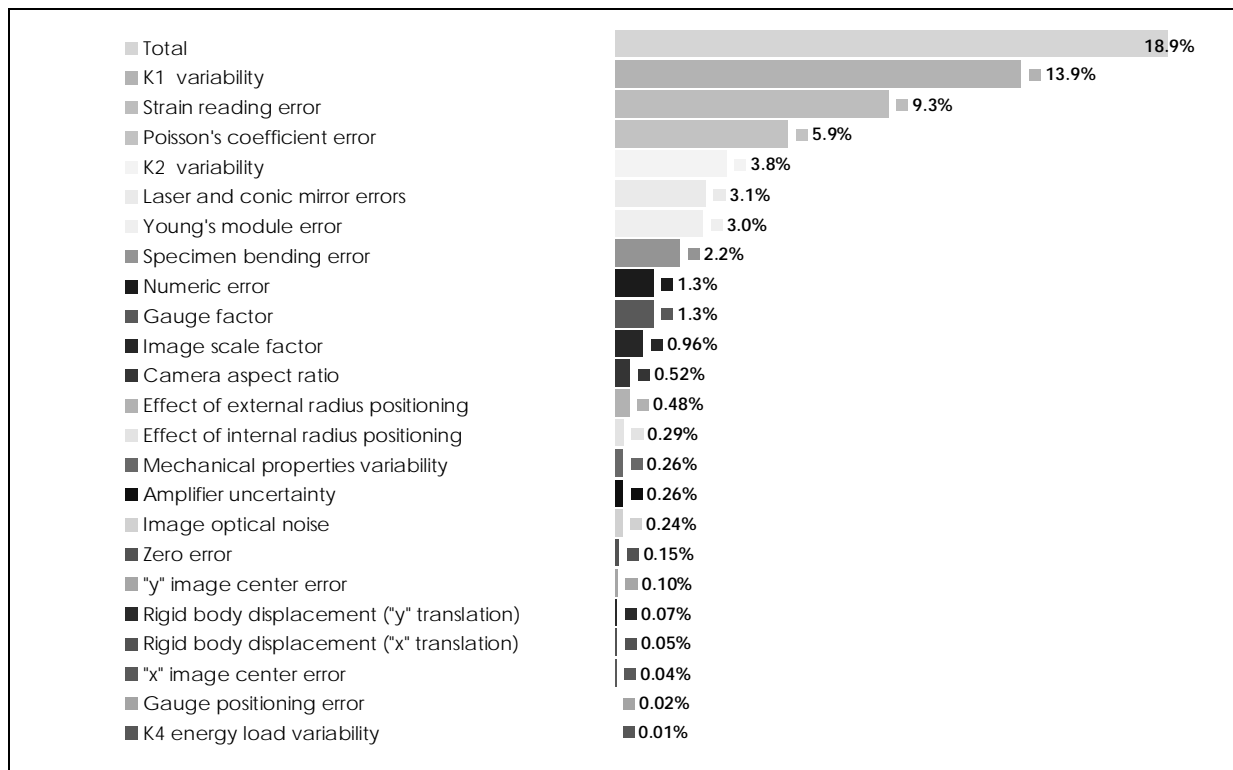
Figure 10: Uncertainty contributions for each analyzed factor for a 177 MPa induced residual stresses and a 2.5 mm diameter spherical indentation tip.

CONCLUSIONS

This paper investigates the possibility to quantify residual stresses combining the indentation method with a radial in-plane electronic speckle pattern interferometer. The hole-drilling mathematical model was taken as a starting point and modified by introducing three unknown parameters: K_1, K_2 and K_3. A set of well controlled experiments was planned to correlate these parameters with the amount of applied residual stresses induced by a mechanical device. Experimental data were analyzed and a quadratic polynomial was fitted to found a relationship between the residual stresses levels and the parameters K_1 and K_2. This polynomial was then used to predict residual stresses from the values of K_1 and K_2 fitted from the measured radial displacement field.

It is clear that K_1 and K_2 in Table 3 are very good choices to be correlated with the residual stresses sum and differences respectively. The term K_3 seams to be more correlated to the indentation energy, and perhaps with local material's hardness. Both conic and spherical indentation tips shows about the same behavior. The values for K_1 and K_2 are obviously different for each indentation tip. Different conical angles or sphere radius must produce different values for K_1 and K_2. For the two tips investigated in this paper it was noted that the sensitivity for the spherical tip is higher than for the conical tip, that means that a larger number of fringes is obtained for the same amount of residual stresses. The experimental data dispersion was smaller for the spherical tip. In addition, the amount of damage in the measured material's surface is smaller if a spherical tip is used. So, spherical tips look to be a better choice.

Best results were found for stresses levels higher than 20% of the material's yield stress. In this work only stresses levels below 80% of the yield stress were investigated. The maximum deviation between the predicted and reference stresses values are of about 8% for the spherical tip in the range of 20% to 80% of the yielding stresses. For the conical tip the difference was about the same, except for an outlier point the reached a difference of 17%. Since only a one-axis stresses state was applied to the specimen, it was not possible to individually verify the dependence of K_1 and K_2 with

the sum and difference between the principal stresses respectively. Although, since the absence of principal stresses difference produces only an axis-symmetrical phase difference pattern, it is clear that the principal stresses difference is responsible for introducing a dependence in terms of $cos(2\theta)$, what is only related to K_2. So, K_1 is not affected by the principal stresses differences. It has to be clear that these results are not definitive. Only one material was involved, only one-axis residual stresses induced was analyzed, only one energy level was used for the indentation.

Further work will be focused on extending those conditions. Different materials and different residual stresses states are currently been investigated. The final goal of this research work is to develop a portable residual stresses measurement unit. The authors believe that the combination of indentation and this radial in-plane ESPI interferometer can be the basis for a very practical device.

ACKNOWLEDGMENTS

REFERENCES

[1] ALBERTAZZI JR, A.; KANDA, C; BORGES, M. R.; HREBABETZKY, F. - *"Portable Residual Stresses Measurement Device Using ESPI and a Radial In-Plane Interferometer"* - Laser Metrology for Precision Measurement and Inspection in Industry; Albertazzi Jr., A.; Eds., Proc. SPIE, v. 4420, p. 112-122, Sep. 2001.

[2] GIANNAKOPOULOS, A. E.; SURESH, S. - *"Indentation of Solids with Gradients in Elastic Properties. Part I: Point Force"* - Journal of Solids and Structures, v.34, n.19, p.2357-2392, 1997.

[3] GIANNAKOPOULOS, A. E.; SURESH, A. - *"Theory of Indentation of Piezoelectric Materials"* - Elsevier Science Ltd., Acta Materialia, v.47 n.7 p.2153-2164, 1997.

[4] LU, JIAN - *"Handbook on Measurement of Residual Stresses"* - The Fairmont Press, SEM - Society for Experimental Mechanics, GA, USA, 1996.

[5] MAKINO, A.; NELSON D. - *"Residual-Stress Determination by Single-Axis Holographic Interferometry and Hole Drilling. Part I: theory"* - Exp. Mech. 34, 66-78 (1994).

[6] SUTERIO, R. - *"Residual Stress Measurement Using Indentation and Electronic Speckle Pattern Interferometry"* (in Portuguese) Doctoral Thesis, Mechanical Engineering Department, UFSC - Federal University of Santa Catarina, 23 Mar., 2005.

[7] SUTERIO, R.; ALBERTAZZI JR., A. G.; AMARAL, F. K., PACHECO, A. - *"Residual Stress Measurement Using Indentation and a Radial In-plane ESPI Interferometer"* – Laser Metrology 2005, 8th International Symposium on Laser Metrology, Macro, Micro, and Nano-Technologies Applied in Science, Engineering, and Industry, Merida, Mexico, 14-18 Feb., 2005.

[8] SUTERIO, R; ALBERTAZZI JR., A. G.; AMARAL, F. K.; - *"Residual Stress Measurement using Indentation and a Radial ESPI Interferometer – Recent Progress"* - ICEM12- 12th International Conference on Experimental Mechanics, Politecnico di Bari, Italy, 29 August - 2 September, 2004.

[9] SUTERIO, R.; ALBERTAZZI JR., A. G.; PACHECO, A.; FERREIRA, R. P. - *"Metrology Analysis of a Simulation Device for Residual Stress"* (in Portuguese) - METROLOGIA 2003 – Brazilian Congress of Metrology, SBM - Brazilian Society of Metrology, Recife, PB, Brazil, sep. 1-5 , 2003.

[10] SUTERIO, R; ALBERTAZZI JR., A. G.; CAVACO, M. A. M. - *"Preliminary Evaluation: The Indentation Method Combined with a Radial Interferometer for Residual Stress Measurement"* - SEM Annual Conference and Exposition on Experimental and Applied Mechanics, SEM - Society for Experimental Mechanics, Charlotte, North Carolina, USA, June 2-4, 2003.

[11] UNDERWOOD, J. H. - *"Residual Stress Measurement using Surface Displacements around an Indentation"* - Experimental Mechanics, p. 373-380, Sep., 1973.